



High nitrate removal by ZnO/AgI nanophotocatalyst using graphene-based compounds

Mahnoush Malmir^a, Amir Mosayebi^b, Mojgan Sheikhpour^{c,d,*}

^aFaculty of Chemical Engineering, North Tehran Branch, Islamic Azad University, Tehran, Iran, email: mahnoush.malmir@yahoo.com (M. Malmir)

^bDepartment of Chemical Engineering, Tafresh University, P.O. Box 79611-39518, Tafresh, Iran, email: mosayebi@tafreshu.ac.ir (A. Mosayebi)

^cDepartment of Mycobacteriology and Pulmonary Research, Pasteur Institute of Iran, Tehran, Iran, Tel. +98-9122969712, +98 21 64112285, Fax +98 21 64112313, email: m_sheikhpour@pasteur.ac.ir, mshaikhpour@gmail.com (M. Sheikhpour)

^dMicrobiology Research Center (MRC), Pasteur Institute of Iran, Tehran, Iran

Received 7 January 2019; Accepted 5 June 2019

ABSTRACT

The nitrate pollution of groundwater and surface water resources is a major environmental problem. The high amounts of nitrate in water can cause the formation of carcinogenic nitrogen-containing organic compounds, such as nitrosamines. In this study, the nitrate removal from the water was studied using ZnO/AgI graphene-based nanophotocatalyst. ZnO/AgI graphene-based nanophotocatalyst was characterized by XRD, BET, EDS, and SEM. The effects of nitrate concentration (60, 100 and 140 ppm), nanophotocatalyst concentration (0.5, 1 and 1.5 g), and pH (4, 6 and 8) were evaluated in visible light and UV light. In the optimal conditions, the highest amount of nitrate removal by ZnO/AgI graphene-based nanophotocatalyst in visible light was found as much as 77% and 97% in UV light. The experiments showed that the nitrate removal of the nanophotocatalyst was increased under the UV light. The result indicates that ZnO/AgI graphene-based nanophotocatalyst can remove nitrate with high percentage; so, it can be the right choice for the degradation of nitrate from water.

Keywords: Nitrate; Graphene; Nanophotocatalyst; UV light

1. Introduction

Nowadays, due to the uncontrollable evacuation of damaging compounds to water, air, soil, and all kinds of lifestyles on earth are very threatening. Also, due to the rapid industrialization and increase of the world population over the past years, a lot of toxic chemicals have been distributed into the environment. Many of these biological, organic and inorganic contaminants have been discovered on the surface, sewage, ground and drinking water. During the past years, the removal of these contaminants has been surveyed [1]. Among those contaminants, nitrate is the first concern on a universal scale, because of its inten-

sive release of nitrate from both industrial and agricultural activities [2].

Human beings have suffered from many health problems such as diarrhea, vomiting, high blood pressure, respiratory tract infections, spontaneous miscarriages and the 'blue baby' syndrome or methemoglobinemia with high intake of nitrate from water. The allowed amounts of nitrate in water have been specified in most of the countries, to prevent these health problems. The maximum amount of NO_3^- for drinking water, appointed by the World Health Organization, is 50 mg/L (11.3 mg N/L), and Australia's maximum NO_3^- limit is 50 mg/L for kid up to three months old; while for adults and children over the age of three months, it is 100 mg/L [3]. Except for the health subject, the high concentration of nitrate in rivers and lakes could create environmental problems such as eutrophication [4]. For finding the drinking water standard, different processes

*Corresponding author.

have been extended for nitrate reduction, including the catalytic reduction, photocatalytic reduction, ion exchange, electrodialysis, reverse osmosis, and biological methods. Among those, one of the most promising techniques, which provide a decrease in dangerous pollutants from our environment, is the photocatalytic degradation.

The outstanding properties of ZnO such as an appropriate band gap (-3.37 eV), high exciting binding energy (60 meV) [5], physical and chemical stability, nontoxicity, the ability to form in different morphologies and inexpensive production cost have caused more attention to the ZnO-based photocatalysts applications [6–10]. However, the attempts to use the bare ZnO as a photocatalyst are encountered with some barriers such as low activity, especially in the visible light wavelengths and rapid recombination of photo-excited electron-hole pairs [11]. Doping ZnO with Fe [12], Co [13], Cu [14] and other transition metals [15–17] could significantly improve the ZnO photocatalytic activity, by increasing the light absorption in the visible light range.

New research works have been assigned to better controlling the recombination level of the photo-excited pairs by hybridizing ZnO with graphene [18–21]. In such hybrids, graphene can act as an excellent electron acceptor with superior electrical conductivity, active surface area, and high visible light optical transparency [22–25]. Such exclusive properties of graphene have encouraged its use in the ZnO-based nanomaterials to increase its photocatalytic activity meaningfully. Regarding this issue, Xu et al. [26] studied the significant effect of graphene with different amounts on graphene-ZnO hybrid photocatalytic activity. Furthermore, Zhai et al. [27] reported the fabrication of graphene-encapsulated ZnO microspheres and synergic effects of graphene on the photocatalytic performance of the composites.

Silver halides are photosensitive materials which can absorb photons in the visible area to make electron-hole pairs. These materials have been used widely in photographic films [28,29]. The high price of silver halides limits their applications in the large-scale photocatalytic processes. Hence, to increase their use in large-scale, one can create nanocomposites between the low-cost semiconductor and silver halides which reduce the cost of the prepared photocatalysts. In recent years, a lot of attention has been paid to the formation of nanocomposite with ZnO and TiO_2 with different silver halides [30–37]. Whereas, the study of photocatalytic activity for AgI/ZnO nanocomposites has rarely been reported [38,39]. Vignesh et al. [39] prepared nanoparticles of ZnO, synthesized with AgI, by a three-step deposition-precipitation method. Then, their activities for photodegradation of rosaniline hydrochloride dye were studied under the visible-light irradiation.

The main goal of this work is to develop a novel graphene-based nanophotocatalyst for better nitrate removal. ZnO/AgI graphene-based nanocomposites exhibited high photodegradation activity for nitrate under visible light and UV irradiation, compared to ZnO nanostructures. Since there was no report of nitrate photocatalytic reduction by ZnO/AgI graphene-based nanocomposites up to now; we conducted it as a novel work. ZnO/AgI graphene-based nanocomposites was used as the photocatalyst. Also, for the first time, the effective operating parameters were optimized in nitrate reduction in the presence of visible and UV light with the response surface methodology. The results

showed that the photocatalytic reduction of nitrate could be performed successfully with this structure of nanocomposite. The morphology, microstructure, specific surface area and purity of ZnO/AgI graphene-based composites were studied using the scanning electron microscopy (SEM), the X-ray diffraction (XRD), the Energy-dispersive X-ray spectroscopy (EDS) and the Brunauer–Emmett–Teller (BET) methods.

2. Materials and methods

2.1. Materials

Zinc nitrate, graphene, silver nitrate, potassium iodide, ethylenediamine, methanol, benzoic acid, salicylaldehyde ($\text{C}_7\text{H}_6\text{O}_2$), and potassium nitrate were supplied from Merck, and distilled water was used for the experiments.

2.2. Synthesis of nanophotocatalyst

The graphene/zinc oxide composite was designed and synthesized by the in-situ thermal decomposition of zinc acetate. The composite exhibited high crystalline quality with the polycrystalline hexagonal wurtzite crystal structure of zinc oxide and amorphous graphene. More importantly, the decomposition mechanism and low-cost strategy, presented here, could be easily extended to the fabrication of graphene with other semiconductor oxide composites [40]. The initial solution was prepared by dissolving one mmol ethylenediamine in 20 mL methanol, then, two mmol salicylaldehyde was dissolved in 50 ml methanol, and the solution of ethylenediamine was added to it drop-by-drop. Finally, refluxed the solution containing the yellow sediment was refluxed for one day, and the resulting yellow sediment was washed with methanol several times. For the synthesis of Zn salen complex, one mmol zinc nitrate salt was dissolved in methanol, and then, two mmol solved salen was added in methanol, in the solution of zinc nitrate. Then, the prepared yellow complex was refluxed for 24 h. For the synthesis of ZnO, 0.5 g of Zn (salen) complex was put in the oven at 500°C for 9 h.

At the end of the synthesis of ZnO-AgI-G, 1 g graphene in 20 ml of water was distributed in the ultrasonic homogenizer for 20 min. Then, 0.5 g of zinc oxide was added to the mixture in an ultrasonic homogenizer. After that, 0.2 g of silver nitrate was added to the mixture too, after 15 min, 0.197 g of potassium iodide, dissolved in water, was added to the mixture, drop-by-drop. The obtained sediment was centrifuged and dried at 60°C for 8 h.

2.3. Analysis and characterizations

The determination of the crystallinity of the samples was studied by the X-Ray Diffraction (XRD). The surface morphology of the nanocomposite was investigated by the scanning electron microscopy (SEM). The surface elemental compositions of the prepared photocatalysts were investigated by energy dispersive X-ray spectroscopy (EDS), and the specific surface was determined by BET for determining the total surface area (reactive surface); note that all the porous structures adsorb the small gas molecules.

2.4. Nitrate and nitrite analysis

To measure the amount of nitrate, we used the chromotropic acid method. In this method, the reaction between Nitrate Reagent A and Nitrate Reagent B with nitrate is created a yellowish solution; then, with a spectrophotometer at 410 nm, the amount of absorption was measured for the resulting solution. Finally, the spectrophotometer data and changes in the absorption were compared with the standard curve, and the concentration of nitrate was absorbed. To measure the amount of nitrite the USEPA Diazotization method was used. The scope of this method for nitrite according to nitrogen was 0.002–0.3 mg/L. In this method, different concentrations of nitrate solution were prepared using sodium nitrite, when nitrite reacted with sulfamic acid; diazonium salt was produced with a pink color. Then, the sample absorption was read with the spectrophotometer at the wavelength of 507 nm; finally, the spectrophotometer data and changes in the absorption were compared with the standard curve, and the nitrite concentration was absorbed.

2.5. Experimental design

The Design-Expert and the response surface methodology were used for the optimization of the nanophotocatalyst denitrification activity. Three variables including the nanophotocatalyst concentration (0.5, 1 and 1.5 g), the pollutant concentration (60, 100 and 140 ppm), and pH (4, 6 and 8) were studied for the optimization. For three variables, according to the experimental design, 15 experiments were determined. The nanophotocatalyst was added to the reactor, and a nitrate test kit determined the amount of nitrate elimination. Then, during 5 h in various concentrations of nitrate and nanophotocatalyst at the pH of 4, 6 and 8, the samples were taken from the reactor, and the nitrate destruction activity was evaluated.

2.6. Reactor

The nitrate destruction activity was investigated in a bubble column with a length of 35 cm and the inner diameter of 10 cm. In this column, a tube was applied with a length of 41 cm and a diameter of 2 cm to locate the lamp and sparger. Also, the reactor included an outlet port, through which, the sampling was carried out. An 8-W fluorescent lamp with a wavelength of 400–700 nm was placed in the reactor tube to examine the degradation of nitrate in visible light, and an 8 W UV-C lamp with the wavelength of 100–280 nm was used for destructing the contaminants in the UV light. The samples were taken every half hour for 5 h. Fig. 1 shows the bubble column.

3. Results and discussion

3.1. SEM analysis

The surface morphology of the ZnO/AgI/graphene nanocomposites was studied by SEM, as illustrated in Fig. 2. Figs. 2a, b, and d show the surface of ZnO/AgI/graphene nanocomposite with a magnification of 20,000 times. Also,



Fig. 1. The structure of the designed reactor.

Fig. 2c reveals the surface of nanocomposite with a magnification of 40,000 times. The figure also shows a surface containing nanoparticles with the diameters ranging from –21 to 70 nm.

3.2. EDS

The EDS analysis was carried out to probe the elemental composition of nanoparticles. As shown in Fig. 3, the various well-defined peaks of Zn, O, C, I and Ag on the surface of nanoparticles confirm the existence of ZnO-AgI nanoparticles on graphene base. Also, the apparent concentration, percentage by weight (wt%), Atomic percentage and a few other parameters of each element extracted from EDS spectra are listed in Table 1.

3.3. XRD

The XRD pattern of ZnO/AgI graphene-based nanocomposite is shown in Fig. 4. The peaks appear at the 2θ values of 22.43, 23.76, 25.45, 32.83, 39.25, 42.58, 45.68, 46.37, 54.53, 56.72, 61.77, 62.31, 71.08, 73.32 and 76.13 are respectively assigned to (100), (111), (101), (102), (110), (103), (210), (321), (300), (213) and (302) diffraction planes of hexagonal and cubic which confirm the formation of AgI nanoparticle. One peak that appears at approximately $2\theta = 26.48^\circ$, which is generally attributed to the (002) diffraction plane

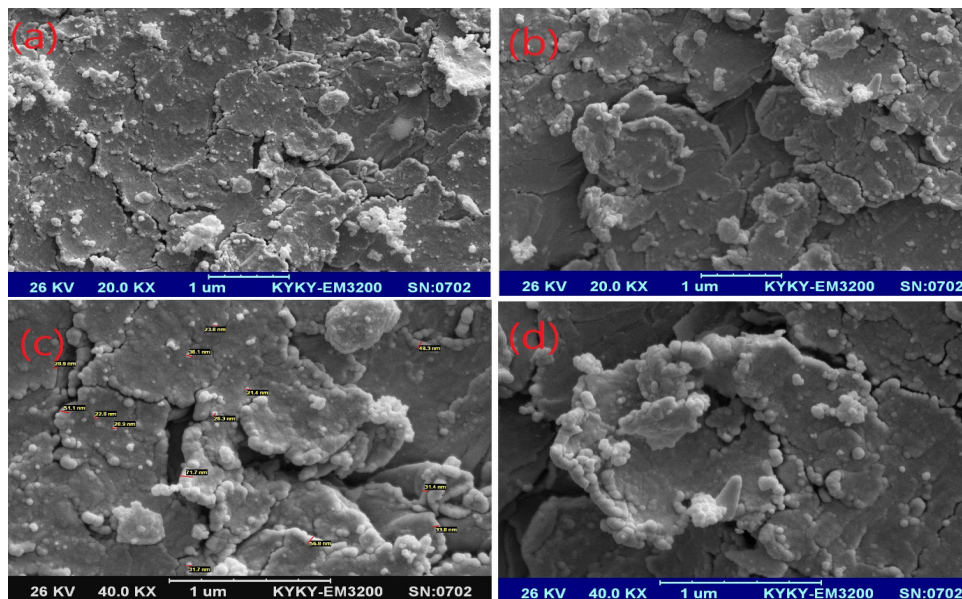


Fig. 2. (a)-(b)-(d) SEM images of ZnO/AgI graphene-based nanocomposite with magnification of 20,000 times, (c) SEM image of ZnO/AgI graphene-based nanocomposite with magnification of 40,000 times.

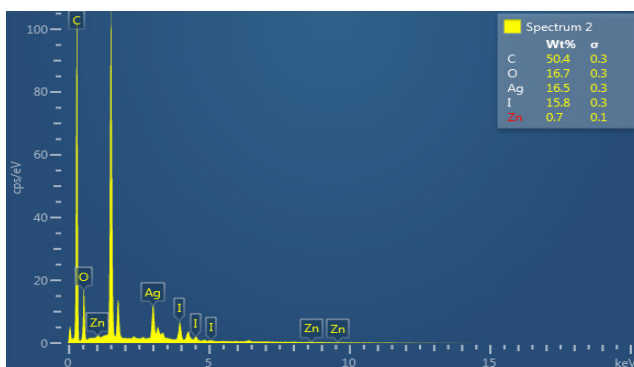


Fig. 3. EDS analysis of ZnO/AgI graphene-based nanocomposite.

of graphene. There is no characteristic peak of ZnO in XRD patterns which is ascribed to a low amount of ZnO. No other diffraction peaks are distinguished, showing the nanoparticles have been successfully synthesized without any impurity phases.

3.4. BET

The active-surface of ZnO/AgI graphene-based the BET test measured nanophotocatalyst. The obtained results are shown in Table 2; also, and Fig. 5 shows the absorption and desorption diagrams of nanophotocatalyst.

3.5. Analysis of engineering parameters in the reactor

In this study, we examined all the hydrodynamic and mass transfer factors and obtained the engineering parameters. The inflow pattern based on agitation, and aeration amount the best flow regime was bubbly and the best aeration amount was 0.17 (vvm). The best mixing time was 20 s

(aeration amount = 0 vvm) at different aeration amounts. After the evaluation of the gas hold up and bubble diameter at different aeration amount, the best amounts of gas hold up, and bubble diameter were obtained as 0.1 (ϵ_g) and 0.1 (mm) when the aeration amount was 0.17 (vvm). Finally, the best amount of mass transfer coefficients ($k_L a$) was obtained as 0.2 in 0.17 (vvm). Tables 3, 4, 5 and 6 show the amount of these values.

3.6. Analysis of nitrate removal

In this study, in the beginning, the nitrate removal was investigated in the absence of nanophotocatalyst, but in the presence of visible light and UV light for 300 min. The results of nitrate removal were evaluated in the visible light and UV light at the room temperature, with the concentration of the pollutants of 100 ppm and pH = 6, after 5 h by using the nitrate test kit. As shown in Fig. 6 the amount of the nitrate removal in the absence of nanophotocatalyst, but in the presence of visible light, was 0%; while that was 6% in the exposure of UV light.

3.7. Optimization of nitrate removal by ZnO/AgI graphene-based nanophotocatalyst

The experiments were designed by the response surface methodology. Responses 1 and 2 were for the checking of nitrate removal percentage. All the experiments were repeated three times, and their averages were provided in the study. The optimization of the effective factors for the nanophotocatalyst is specified in Table 7.

The data analysis was performed according to the obtained responses by using the Design-Expert software and the response surface methodology. It should be noted that A is a variable which represents the pH, B is a variable which represents the pollutant concentration, and C is a

Table 1
Elements ratio of ZnO/AgI graphene-based nanocomposite extracted from EDS spectra

Element	Line type	Apparent concentration	k ratio	Wt%	Wt% Sigma	Atomic %	Standard label	Factory standard
C	K series	18.54	0.18541	50.40	0.33	75.92	C Vit	Yes
O	K series	6.59	0.02219	16.70	0.26	18.88	SiO ₂	Yes
Zn	L series	0.16	0.00155	0.68	0.13	0.19	Zn	Yes
Ag	L series	6.30	0.06303	16.45	0.29	2.76	Ag	Yes
I	L series	5.39	0.05394	15.76	0.29	2.25	I (v)	Yes
Total:				100.00		100.00		

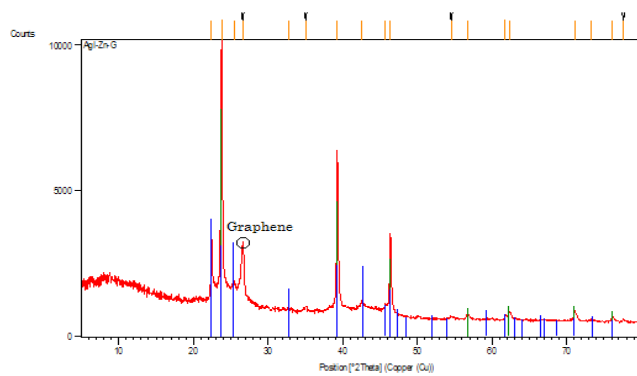


Fig. 4. X-ray diffraction pattern of ZnO/AgI based on graphene.

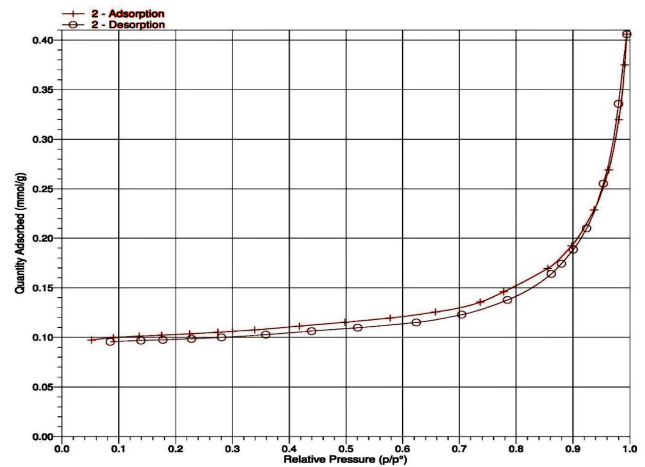


Fig. 5. Isotherm linear plot of ZnO/AgI graphene-based nanophotocatalyst.

Table 2
The measured parameters of ZnO/AgI graphene-based nanophotocatalyst by BET test

Parameter	Reported amount
BET surface area (m ² /g)	21.61
BJH adsorption average pore width (nm)	16.50
BJH desorption average pore width (nm)	22.90
BJH adsorption cumulative volume of pores (cm ³ /g)	0.086
BJH desorption cumulative volume of pores (cm ³ /g)	0.083
Adsorption average pore diameter (nm)	6.91
Desorption average pore diameter (nm)	8.40

variable which represents the concentration of nanophotocatalyst. Tables 8 and 9 show the responses R1 and R2 for nanophotocatalyst.

The influencing parameters are the factors with the p-value less than 0.1. Therefore, the following factors are important and effective in the responses R1 and R2 for the nanophotocatalyst. As a result, the final equations for R1 and R2 are:

$$R1 = +0.78 - 0.045 \times A + 0.069 \times C - 0.12 \times A^2 - 0.19 \times B^2 - 0.082 \times C^2 \quad (1)$$

$$R2 = +0.99 - 0.035 \times A + 0.070 \times C - 0.12 \times A^2 - 0.26 \times B^2 - 0.14 \times C^2 \quad (2)$$

Table 3
The flow pattern based on agitation and aeration amount

Flow regime	Aeration/amount (vvm)
Slug	0
Slug to bubbly	0.17
Slug	0.4
Slug to bubbly	0
Bubbly	0.17
Slug	0.4
Slug	0
Slug	0.17
Slug	0.4

Table 4
Evaluation of mixing time at different aeration amounts (vvm)

Mixing time (s)	(vvm) aeration amount
20	0
10	0.17
15	0.4

Table 5
Evaluation of the gas hold up and diameter bubble at different aeration amounts (vvm)

Gas hold up (ϵ_g)	Bubble diameter (mm)	(vvm) aeration amount
0.02	0.4	0
0.1	0.1	0.17
0.05	0.15	0.4

Table 6
Mass transfer coefficients ($k_L a$) and aeration

$k_L a$	Aeration amount (vvm)
0.02	0
0.2	0.17
0.1	0.4

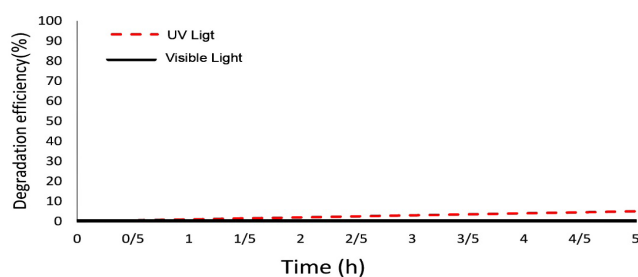


Fig. 6. Nitrate removal in the absence of nanophotocatalyst.

According to Eq. (1), the optimal conditions of R1 for the nanophotocatalyst are as $A = 0.07$, $B = -0.28$ ppm, $C = 0.38$ g and $R1 = 0.774017$. Also, according to Eq. (2), the optimal conditions of R2 for the nanophotocatalyst are as $A = -0.41$, $B = 0.23$ (ppm), $C = 0.05$ (g) and $R2 = 0.972361$. Regarding the relationship between Eq. (1) and the optimal conditions of R1, and Eq. (2) with the optimal conditions of R2, Fig. 7 shows the two-dimensional diagram of the responses R1 and R2. Fig. 7a shows the optimum conditions for the nanophotocatalyst in visible light, while Fig. 7b shows the optimum conditions for the nanophotocatalyst in UV light.

As shown in Fig. 7a, by increasing of the parameter A to 0 (pH = 6) and reducing of the parameter B to -1 (60 ppm), the amount of R1 increases; which is equivalent to increasing the percentage of the nitrate removal. In this study, the range of pH = 4 to pH = 8 was investigated in the nitrate removal, and the highest photocatalytic removal in visible light was achieved in pH = 6, over 5 h (Table 7). The results clearly show that this ZnO/AgI graphene-based nanophotocatalyst has a strong photocatalytic degradation ability in a wide range of pH. As mentioned in Table 7, with increasing of the nanophotocatalyst concentrations, the nitrate removal rate increases. Increasing the concentrations of the nanophotocatalyst causes an increase in the possibility of collision between the nitrate and nanoparticles [41].

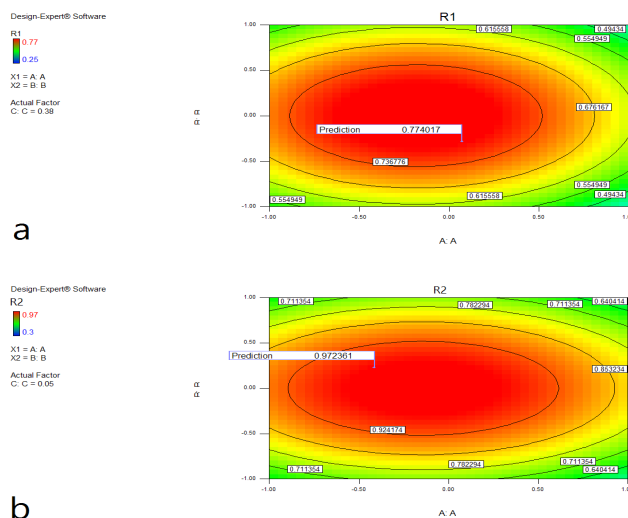


Fig. 7. The interaction of A and B parameters in a two-dimensional diagram of (a) in visible light and (b) in UV light.

Table 7
Experimental results for ZnO/AgI/graphene based on the statistical program (nitrate removal in visible light)

pH	Nitrate concentration	Nano photocatalyst concentration	Nitrate degradation efficiency (UV)	Nitrate degradation efficiency (visible light)
-1	-1	-1	42%	37%
1	-1	-1	33%	25%
-1	1	-1	39%	31%
1	1	-1	30%	25%
-1	-1	1	53%	44%
1	-1	1	53%	42%
-1	1	1	62%	58%
1	1	1	52%	41%
-1	0	0	93%	71%
1	0	0	86%	63%
0	-1	0	72%	59%
0	1	0	79%	61%
0	0	-1	91%	70%
0	0	1	85%	72%
0	0	0	97%	74%
0	0	0	97%	76%
0	0	0	97%	73%
0	0	0	97%	75%
0	0	0	97%	77%
0	0	0	97%	77%

3.8. ZnO nanoparticles performance in optimized conditions and visible light and UV light

The ZnO nanoparticles performance was investigated under the optimized conditions, under the visible and UV light. The effective parameters were achieved for the

Table 8
Response R1 for ZnO/AgI/graphene nanophotocatalyst in visible light

Term	Sum of Sq.	Df	Mean Sq.	F value	p-value
A-A	0.020	1	0.020	12.73	0.0031
C-C	0.048	1	0.048	29.94	0.0001
A ²	0.041	1	0.041	25.85	0.0002
B ²	0.10	1	0.10	63.93	0.0001
C ²	0.019	1	0.019	11.70	0.0041
R-Squared	0.9640				

Table 9
Response R2 for ZnO/AgI/graphene nano-photocatalyst in UV light

Term	Sum of Sq.	Df	Mean Sq.	F value	p-value
A-A	0.012	1	0.012	4.16	0.0607
C-C	0.049	1	0.049	16.65	0.0011
A ²	0.042	1	0.042	14.39	0.0020
B ²	0.19	1	0.19	65.17	0.0001
C ²	0.053	1	0.053	18.08	0.0008
R-Squared	0.9640				

Table 10
The optimal conditions for ZnO under visible light

Type of irradiation	A	B (ppm)	C (g)	Nitrate degradation efficiency
Visible light	0.07	-0.28	0.38	%15
UV light	-0.41	0.23	0.05	%26

nanoparticles, which are shown in Table 10. In this condition, ZnO was able to remove 15% of the nitrate under visible light, and 26% under UV light.

3.9. Photocatalytic activity

The photocatalytic efficiency of the nanocomposite was examined by their activity for nitrate degradation. The ZnO/AgI graphene-based nanocomposite, especially the UV-treated ones, could degrade nearly all the nitrate of the solution in the bubble column after 300 min of UV irradiation. But, under the visible light irradiation, the nanocomposite could degrade only ~77% at the same experimental conditions.

3.10. Photocatalytic mechanism

The photocatalytic process involves many competing reactions. The widely proposed photodegradation mechanism for graphene base nanophotocatalyst has been shown in Fig. 8. when photocatalyst surface is exposed to the light with sufficient energy, equal or larger than the band gap, the electron-hole pairs are generated [42]. The band gap of AgI is 2.8 eV which is lower than that of ZnO (3.2 eV) [43,44]. Absorption of a photon with energy greater than the band gap energy of AgI under visible light irradiation ($\lambda \geq 400$ nm), the electrons in the valence band (VB) of AgI can be excited to the conduction band (CB), and the holes are left in the VB [Eq. (3)]. Because the CB energy of AgI (-0.42 eV) is more negative than that of ZnO (-0.34 eV) [43,44], the photoexcited electrons in the CB of AgI can be easily injected into the CB of ZnO [Eq. (4)] [45]. These photogenerated electrons tend to transfer to graphene sheets and then scavenged by dissolved oxygen, facilitating the electron-hole separation. Meanwhile, the holes can either react with adsorbed water (or surface hydroxyl) to form hydroxyl radicals or directly oxidize various organic compounds. The major reaction steps in this nano photocata-

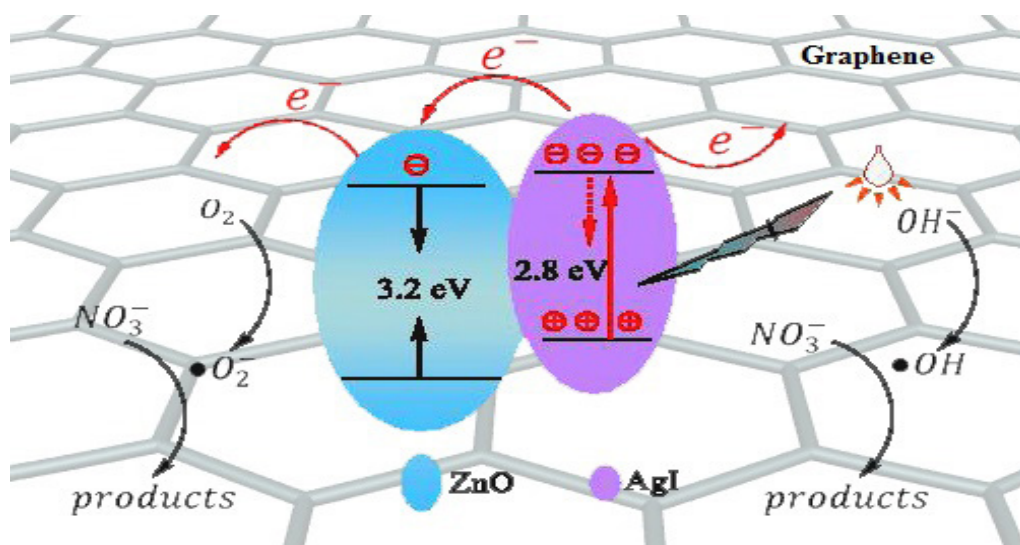
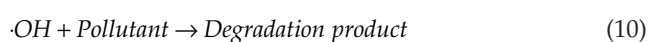
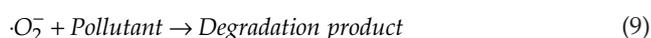
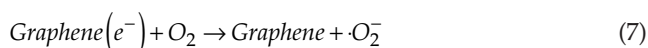
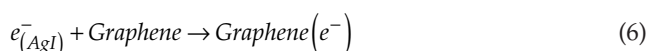
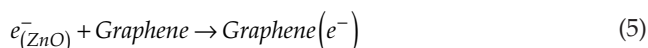


Fig. 8. Schematic illustration of high photocatalytic activity of ZnO/AgI nanophotocatalyst on graphene used as a conducting support.

lytic degradation mechanism under UV-light irradiation are summarized by the following equations [46].



3.11. Nitrate removal kinetics in the optimum conditions

The kinetics of nitrate removal was investigated in the optimum conditions for 5 h, and the results graph was plotted. The kinetic results of nitrate removal by ZnO/AgI graphene-based nanophotocatalyst show that, as time passes, the percentage of nitrate degradation is increased. The peak of this increase is seen after 5 h, and then, there is no increase. Fig. 9. indicates that the required time would be 5 h to achieve balance conditions and maximum removal.

To compare these results with published articles a summary of adsorption capacities of various adsorbents for nitrate removal are listed in Table 11.

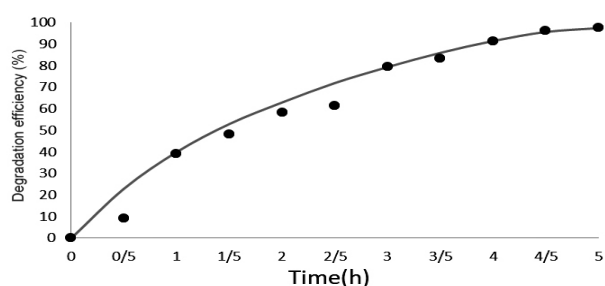


Fig. 9. Kinetics of the nitrate removal in the optimal condition.

4. Conclusions

In this study, a novel and effective ZnO/AgI graphene-based nanophotocatalyst was created for the nitrate removal with high selectivity. ZnO/AgI graphene-based nanophotocatalyst was successfully prepared using the thermal decomposition method, which had more advantages over the other methods for the simple manufacturing process and high purity of the products. The nitrate destruction activity was investigated in a bubble column. An 8-W fluorescent lamp with a wavelength of 400–700 nm was placed in the reactor tube to examine the degradation of nitrate in visible light, while an 8 W UV-C lamp with the wavelength of 100–280 nm was used for destructing the contaminants in UV light. The structure of the nanophotocatalyst was investigated by the XRD, SEM, and BET analyses. Also, the photocatalytic activity of ZnO/AgI graphene-based nanophotocatalyst was investigated by the degradations of nitrate under the UV light and visible-light irradiation.

It was found that the photocatalytic activity of nanophotocatalyst depended on the pH, contaminant concentration and nanophotocatalyst concentration. The average amount of these variables is the best value. This amount is the photocatalytic concentration of 1 g, the nitrate concentration of 100 ppm, and the pH of 6. The pH is one of the parameters which affect the activity of nitrification, as mentioned in previous studies. In the optimal conditions, the highest amount of nitrate removal by ZnO/AgI graphene-based nanophotocatalyst in visible light was found as 77%, and 97% under the UV light. It was observed that the photocatalytic activity increased under the UV light irradiation. These results could provide new knowledge for solving the nitrogen removal problems in the sewage effluent treatment and the applications in the nitrate-contaminated water.

References

- [1] A. Pal, Y. He, M. Jekel, M. Reinhard, K.Y.-H. Gin, Emerging contaminants of public health significance as water quality indicator compounds in the urban water cycle, *Environ. Int.*, 71 (2014) 46–62.
- [2] Y. Ding, W. Sun, W. Yang, Q. Li, Formic acid as the in-situ hydrogen source for catalytic reduction of nitrate in water by PdAg alloy nanoparticles supported on amine-functionalized SiO₂, *Appl. Catal. B: Environ.*, 203 (2017) 372–380.
- [3] N. NHMRC, Australian drinking water guidelines paper 6 national water quality management strategy. National Health

Table 11

Adsorption capacities and other parameters for the removal of nitrate by different sorbents

No.	Adsorbent	Maximum nitrate removal (%)	Nitrate concentration (mg/L)	pH	Ref.
1	Nanofiltration	75	35	–	[47]
2	Ag-doped TiO _{2,na} nanoparticle	95.5	100	5	[41]
3	GO blended PSF mixed matrix membrane (GO = 0)	15.5	110	8	[48]
4	GO blended PSF mixed matrix membrane (GO = 0.5 wt%)	22.78	110	8	[48]
5	GO blended PSF mixed matrix membrane (GO = 1 wt%)	39.12	110	8	[48]
6	GO blended PSF mixed matrix membrane (GO = 2 wt%)	41.37	110	8	[48]

- and Medical Research Council, National Resource Management Ministerial Council, Commonwealth of Australia, Canberra, 2011.
- [4] J.A. Camargo, Á. Alonso, Ecological and toxicological effects of inorganic nitrogen pollution in aquatic ecosystems: a global assessment, *Environ. Int.*, 32(6) (2006) 831–849.
 - [5] P. Yang, H. Yan, S. Mao, R. Russo, J. Johnson, R. Saykally, N. Morris, J. Pham, R. He, H.-J. Choi, Controlled growth of ZnO nanowires and their optical properties, *Adv. Funct. Mater.*, 12(5) (2002) 323.
 - [6] M. Ahmad, J. Zhu, ZnO based advanced functional nanostructures: synthesis, properties and applications, *J. Mater. Chem.*, 21(3) (2011) 599–614.
 - [7] O. Akhavan, Photocatalytic reduction of graphene oxides hybridized by ZnO nanoparticles in ethanol, *Carbon*, 49(1) (2011) 11–18.
 - [8] O. Akhavan, M. Mehrabian, K. Mirabbaszadeh, R. Azimirad, Hydrothermal synthesis of ZnO nanorod arrays for photocatalytic inactivation of bacteria, *J. Physics D: Appl. Phys.*, 42(22) (2009) 225305.
 - [9] F. Liu, Y.H. Leung, A.B. Djurišić, A.M.C. Ng, W.K. Chan, K.L. Ng, K.S. Wong, C. Liao, K. Shih, C. Surya, Effect of plasma treatment on native defects and photocatalytic activities of zinc oxide tetrapods, *J. Phys. Chem. C*, 118(39) (2014) 22760–22767.
 - [10] J. Xiao, T. Frauenheim, T. Heine, A. Kuc, Temperature-mediated magnetism in Fe-doped ZnO semiconductors, *J. Phys. Chem. C*, 117(10) (2013) 5338–5342.
 - [11] Z. Chen, N. Zhang, Y.-J. Xu, Synthesis of graphene–ZnO nanorod nanocomposites with improved photoactivity and anti-photocorrosion, *Cryst. Eng. Comm.*, 15(15) (2013) 3022–3030.
 - [12] K. Kumar, M. Chitkara, I.S. Sandhu, D. Mehta, S. Kumar, Photocatalytic, optical and magnetic properties of Fe-doped ZnO nanoparticles prepared by chemical route, *J. Alloys Comp.*, 588 (2014) 681–689.
 - [13] X.-C. Liu, E.-W. Shi, Z.-Z. Chen, H.-W. Zhang, L.-X. Song, H. Wang, S.-D. Yao, Structural, optical and magnetic properties of Co-doped ZnO films, *J. Crystal Growth*, 296(2) (2006) 135–140.
 - [14] Z. Wu, K. Cheng, F. Zhang, R. Guan, X. Wu, L. Zhuge, Effect of Al co-doping on the electrical and magnetic properties of Cu-doped ZnO nanorods, *J. Alloys Comp.*, 615 (2014) 521–525.
 - [15] W.-H. Kim, J.Y. Son, Room temperature magneto resistance of horizontally aligned Mn-doped ZnO nanowires on terrace edges, *Mater. Lett.*, 133 (2014) 101–104.
 - [16] J. Park, G. Park, H.-J. Ko, J.-S. Ha, The effect of ITO/Mo/MoO₃ anode multilayer film on efficient hole extraction in MEH-PPV/ZnO NP hybrid solar cells, *Ceramics Int.*, 40(10) (2014) 16281–16285.
 - [17] K. Shinde, R. Pawar, B. Sinha, H. Kim, S. Oh, K. Chung, Optical and magnetic properties of Ni doped ZnO planetary ball milled nanopowder synthesized by co-precipitation, *Ceramics Int.*, 40(10) (2014) 16799–16804.
 - [18] O. Akhavan, Graphene nanomesh by ZnO nanorod photocatalysts, *ACS Nano*, 4(7) (2010) 4174–4180.
 - [19] B. Li, T. Liu, Y. Wang, Z. Wang, ZnO/graphene-oxide nanocomposite with remarkably enhanced visible-light-driven photocatalytic performance, *J. Colloid Interface Sci.*, 377(1) (2012) 114–121.
 - [20] J. Wang, T. Tsuzuki, B. Tang, X. Hou, L. Sun, X. Wang, Reduced graphene oxide/ZnO composite: reusable adsorbent for pollutant management, *ACS Appl. Mater. Interfaces*, 4(6) (2012) 3084–3090.
 - [21] C. Wen, F. Liao, S. Liu, Y. Zhao, Z. Kang, X. Zhang, M. Shao, Bi-functional ZnO–RGO–Au substrate: photocatalysts for degrading pollutants and SERS substrates for real-time monitoring, *Chem. Commun.*, 49(29) (2013) 3049–3051.
 - [22] K.I. Bolotin, K. Sikes, Z. Jiang, M. Klima, G. Fudenberg, J. Hone, P. Kim, H. Stormer, Ultrahigh electron mobility in suspended graphene, *Solid State Commun.*, 146(9) (2008) 351–355.
 - [23] D. Chen, L. Tang, J. Li, Graphene-based materials in electrochemistry, *Chem. Soc. Rev.*, 39(8) (2010) 3157–3180.
 - [24] D. Li, R.B. Kaner, Graphene-based materials, *Nat. Nanotechnol.*, 3 (2008) 101.
 - [25] M.-Q. Yang, N. Zhang, M. Pagliaro, Y.-J. Xu, Artificial photosynthesis over graphene–semiconductor composites. Are we getting better? *Chem. Soc. Rev.*, 43(24) (2014) 8240–8254.
 - [26] T. Xu, L. Zhang, H. Cheng, Y. Zhu, Significantly enhanced photocatalytic performance of ZnO via graphene hybridization and the mechanism study, *Appl. Catal. B: Environ.*, 101(3) (2011) 382–387.
 - [27] J. Zhai, L. Sun, H. Yu, H. Li, X. Zhang, H. Yang, J. Xu, A facile approach of fabricating graphene-encapsulated ZnO microspheres and their synergic effect on photocatalytic performance, *J. Nanopart. Res.*, 16(6) (2014) 2433.
 - [28] T. Li, Y. He, H. Lin, J. Cai, L. Dong, X. Wang, M. Luo, L. Zhao, X. Yi, W. Weng, Synthesis, characterization and photocatalytic activity of visible-light plasmonic photocatalyst AgBr–SmVO₄, *Appl. Catal. B: Environ.*, 138 (2013) 95–103.
 - [29] D. Wang, Y. Duan, Q. Luo, X. Li, L. Bao, Visible light photocatalytic activities of plasmonic Ag/AgBr particles synthesized by a double jet method, *Desalination*, 270 (2011) 174–180.
 - [30] C. An, W. Jiang, J. Wang, S. Wang, Z. Ma, Y. Li, Synthesis of three-dimensional AgI@TiO₂ nanoparticles with improved photocatalytic performance, *Dalton Trans.*, 42(24) (2013) 8796–8801.
 - [31] K. Dai, J. Lv, L. Lu, Q. Liu, G. Zhu, D. Li, Synthesis of micro-nano heterostructure AgBr/ZnO composite for advanced visible light photocatalysis, *Mater. Lett.*, 130 (2014) 5–8.
 - [32] B. Krishnakumar, B. Subash, M. Swaminathan, AgBr–ZnO–An efficient nano-photocatalyst for the mineralization of Acid Black 1 with UV light, *Separ. Purif. Technol.*, 85 (2012) 35–44.
 - [33] L. Shi, L. Liang, J. Ma, J. Sun, Improved photocatalytic performance over AgBr/ZnO under visible light, *Superlatt. Microstruct.*, 62 (2013) 128–139.
 - [34] C. Wu, L. Shen, Y.C. Zhang, Q. Huang, Synthesis of AgBr/ZnO nanocomposite with visible light-driven photocatalytic activity, *Mater. Lett.*, 66(1) (2012) 83–85.
 - [35] Y. Xing, R. Li, Q. Li, J. Yang, A new method of preparation of AgBr/TiO₂ composites and investigation of their photocatalytic activity, *J. Nanopart. Res.*, 14(12) (2012) 1284.
 - [36] J. Yi, L. Huang, H. Wang, H. Yu, F. Peng, AgI/TiO₂ nanobelts monolithic catalyst with enhanced visible light photocatalytic activity, *J. Hazard. Mater.*, 284 (2015) 207–214.
 - [37] Y. Zang, R. Farnood, Photocatalytic activity of AgBr/TiO₂ in water under simulated sunlight irradiation, *Applied Catal. B: Environ.*, 79(4) (2008) 334–340.
 - [38] J. Lu, H. Wang, Y. Dong, F. Wang, S. Dong, Plasmonic AgX nanoparticles-modified ZnO nanorod arrays and their visible-light-driven photocatalytic activity, *Chinese J. Catal.*, 35(7) (2014) 1113–1125.
 - [39] K. Vignesh, A. Suganthi, M. Rajarajan, S. Sara, Photocatalytic activity of AgI sensitized ZnO nanoparticles under visible light irradiation, *Powder Technol.*, 224 (2012) 331–337.
 - [40] R. Hong, L. Ding, C. Tao, D. Zhang, In situ synthesis of graphene/zinc oxide composite by thermal decomposition of zinc acetate, *Int. J. Nanotechnol.*, 12(10–12) (2015) 811–817.
 - [41] S. Parastar, S. Nasser, S.H. Borji, M. Fazlzadeh, A.H. Mahvi, A.H. Javadi, M. Gholami, Application of Ag-doped TiO₂ nanoparticle prepared by photodeposition method for nitrate photocatalytic removal from aqueous solutions, *Desal. Water Treat.*, 51(37–39) (2013) 7137–7144.
 - [42] F. Hosseini, A. Kasaeian, F. Pourfayaz, M. Sheikhpour, D. Wen, Novel ZnO–Ag/MWCNT nanocomposite for the photocatalytic degradation of phenol, *Mater. Sci. Semicond. Process.*, 83 (2018) 175–185.
 - [43] S. Shaker-Agjeekandy, A. Habibi-Yangjeh, Ultrasonic-assisted preparation of novel ternary ZnO/AgI/Ag₂CrO₄ nanocomposites as visible-light-driven photocatalysts with excellent activity, *Mater. Sci. Semicond. Process.*, 44 (2016) 48–56.
 - [44] S.R. Morrison, *Electrochemistry at semiconductor and oxidized metal electrodes*. 1980.

- [45] H. Huang, N. Huang, Z. Wang, G. Xia, M. Chen, L. He, Z. Tong, C. Ren, Room-temperature synthesis of carnation-like ZnO@AgI hierarchical nanostructures assembled by AgI nanoparticles-decorated ZnO nanosheets with enhanced visible light photocatalytic activity, *J. Colloid Interface Sci.*, 502 (2017) 77–88.
- [46] Q. Xiang, J. Yu, M. Jaroniec, Graphene-based semiconductor photocatalysts, *Chem. Soc. Rev.*, 41(2) (2012) 782–796.
- [47] M. Sancho, S. Álvarez-Blanco, G. Kombo, B. García-Fayos, Experimental determination of nanofiltration models: application to nitrate removal, *Desal. Water Treat.*, 57(48–49) (2016) 22852–22859.
- [48] R. Rezaee, S. Nasser, A.H. Mahvi, R. Nabizadeh, S.A. Mousavi, A. Maleki, M. Alimohammadi, A. Jafari, S. Hemmati Borji, Development of a novel graphene oxide-blended polysulfone mixed matrix membrane with improved hydrophilicity and evaluation of nitrate removal from aqueous solutions, *Chem. Eng. Commun.*, 206(4) (2019) 495–508.